

Paramagnons in FeSe close to a magnetic quantum phase transition: *Ab initio* study

F. Essenberger, P. Buczek, A. Ernst, L. Sandratskii, and E. K. U. Gross
Max-Planck-Institut für Mikrostrukturphysik, Weinberg 2, D-06120 Halle, Germany
 (Received 19 March 2012; published 28 August 2012)

The magnetic excitations in FeSe are studied from first principles applying linear response density functional theory. The position of the selenide layer is varied to model the transition between paramagnetic and antiferromagnetic phases. In the paramagnetic phase, close to the magnetic instability, we find a branch of long-lived collective spin excitations (paramagnons). An estimation of the paramagnon-mediated effective electron-electron interaction supports the scenario of Cooper pairing in FeSe induced by spin fluctuations.

DOI: [10.1103/PhysRevB.86.060412](https://doi.org/10.1103/PhysRevB.86.060412)

PACS number(s): 75.78.-n, 75.30.Ds, 74.20.Mn

Introduction. The discovery of high-temperature superconductivity in $\text{LaFeAsO}_{1-x}\text{F}_x$ (Ref. 1) induced a great deal of experimental and theoretical interest for the iron-based “pnictide” family of superconductors. Among the pnictides the 11 type² has the simplest structure and can be considered as the parent compound of the superconducting arsenide family.² These compounds consist of square planar sheets of Fe with chalcogen atoms (either sulfur, selenium, or tellurium) forming distorted tetrahedrons around the Fe atoms. The electronic structure of the 11 compounds is very similar to the one of Fe-As based superconductors³ which have a much larger chemical unit cell. In the 11 type only FeSe shows superconductivity (SC) without doping. The T_c of FeSe is with 9K rather small, but it is strongly enhanced by pressure ($T_c \approx 37$ K at 2 GPa);⁴ the application of pressure intensifies also the antiferromagnetic (AFM) spin fluctuations,⁵ indicating a connection between spin excitations and superconductivity.

The small unit cell, the similarities to the Fe-As compounds in the electronic structure, and the presence of superconductivity without doping make FeSe an ideal benchmark system to study the Fe-based superconductors. A theoretical approach to superconductivity considering only electron-phonon coupling as the Cooper-pairing mechanism predicts critical temperatures of less than 1K for these materials.⁶ This points to an alternative pairing mechanism present in the family.⁷ A compelling model was suggested by Mazin *et al.*, who considered a pairing mediated by AFM spin fluctuations (SFs).⁷

The present work reports an *ab initio* study of the magnetic excitations in both paramagnetic (PM) and antiferromagnetic phases of FeSe. We show that close to the point of the magnetic phase transition a branch of intense, long-living paramagnons is formed. We analyze the nature of the excitations and make an estimation of an effective electron-electron interaction mediated by these excitations.

Methods. The fluctuations in the PM phase are studied using the longitudinal dynamic spin susceptibility $\chi_{zz}(\mathbf{r}\mathbf{r}'\mathbf{q}\omega)$ describing the spin response of the system to an external magnetic field. Here $\mathbf{q}\omega$ are the wave vector and the frequency of both the applied field and induced magnetization. The vector \mathbf{q} varies within the first BZ and determines the transformation of the quantities under application of the lattice translations. The vectors \mathbf{r} and \mathbf{r}' are inside the unit cell. Note that in a PM system $\chi_{zz} = \chi_{yy} = \chi_{xx}$ and the induced magnetization is always parallel to the external magnetic field. The susceptibility is calculated using linear-response-density-functional theory

(LRDFT)⁸ implemented in a Korringa-Kohn-Rostoker (KKR) multiple scattering code.⁹ To describe the dependence on \mathbf{r}, \mathbf{r}' a basis composed of products of the Chebyshev polynomials and spherical harmonics is used.¹⁰ In the following, the susceptibilities are assumed to be represented by the matrices in this basis. As a first step the noninteracting Kohn-Sham (KS) susceptibility $\chi_{zz}^{\text{KS}}(\mathbf{r}\mathbf{r}'\mathbf{q}\omega)$ is calculated as an autoconvolution of the KKR Green’s function. Then the Dyson equation of LRDFT is solved using the adiabatic local spin density approximation (ALSDA) for the exchange-correlation (xc) kernel $f^{\text{xc}}(\mathbf{r}\mathbf{r}'\mathbf{q}\omega) \approx \delta_{\mathbf{r}\mathbf{r}'} f^{\text{ALSDA}}(\mathbf{r})$:

$$\chi_{zz} = \chi_{zz}^{\text{KS}} + \chi_{zz}^{\text{KS}} f^{\text{xc}} \chi_{zz}. \quad (1)$$

The calculations are performed for complex frequencies, followed by an analytic continuation to the real frequency axis.¹⁰ Finite values of $\text{Im} \chi_{zz}^{\text{KS}}$ indicate the presence of single particle (Stoner) excitations, whereas peaks of $\text{Im} \chi_{zz}$ yield information about energies and lifetimes of collective excitations. In analogy to magnons, the collective excitations in magnetically ordered systems, the collective excitations in PM are referred to as paramagnons. Although the main focus of the Rapid Communication is on the SFs in the PM phase, for the sake of comparison we present also the spectrum of AFM magnons obtained by mapping the system on the Heisenberg Hamiltonian of interacting atomic moments.¹¹

Magnetic excitations. Experimentally FeSe is a PM metal.⁴ The crystal symmetry does not require a specific distance z_{Se} of the Se layers with respect to the Fe layers. Our calculations reveal a very strong dependence of the electronic properties of the system on the value of z_{Se} , which is demonstrated in Fig. 1 by the dramatic variations of the Fermi surface (FS). Also the magnetic state changes from PM at low z_{Se} to AFM at larger values of this parameter. This indicates a proximity of the experimentally observed PM phase to a magnetic state. We use the sensitivity to z_{Se} to investigate the variation of the SFs while approaching the magnetic critical point.

Experimentally¹² also a small ($\frac{b-a}{b} \approx 0.2\%$ for 0.25 GPa) orthorhombic distortion is observed, which is increasing with pressure ($\frac{b-a}{b} \approx 0.7\%$ for 12 GPa). Our test calculations for pressures ranging between 0 and 12 GPa indicate no change in the equilibrium z_{Se} and critical magnetic z_{Se} , if the distortions are taken into account. Hence, all the presented calculations are performed for the tetragonal crystal structure ($a = b$).

The evolution towards the magnetic instability is demonstrated in the map of the static nonuniform KS susceptibility

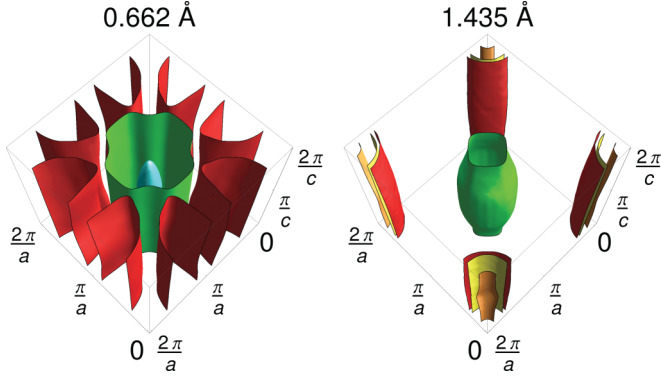


FIG. 1. (Color online) Fermi surface of FeSe for two values of z_{Se} .

calculated for nonmagnetic FeSe. To distinguish the instabilities with respect to the formation of various magnetic structures we consider the Fourier component of the susceptibility, i.e., $\chi_{zz}^{\text{KS}}(\mathbf{Q}) = \int \int d^3r d^3r' e^{-i\mathbf{Q}(\mathbf{r}-\mathbf{r}')} \chi_{zz}^{\text{KS}}(\mathbf{r}\mathbf{r}')$ (Fig. 2). The vector \mathbf{Q} varies both inside ($M \rightarrow X$) and outside ($X \rightarrow G$) of the first BZ of the paramagnetic FeSe. The point Γ ($\mathbf{Q} = 0$) in Fig. 2 corresponds to the FM structure while the points M and G correspond to the antiferromagnetic structures of respectively stripe and checkerboard types (Fig. 3). For small z_{Se} a large magnetic response is obtained for wave vectors close to Γ that specifies strong ferromagnetic fluctuations. With increasing z_{Se} the fluctuations weaken for all \mathbf{Q} values. Nearing the experimental z_{Se} , the susceptibility increases again. This time, however, the increase is strongest around the M point and between the X and G points.

The results of the spin-polarized self-consistent calculations for the stripe and checkerboard magnetic structures are presented in Fig. 3. In agreement with the picture given by the static susceptibility (Fig. 2), the system becomes magnetic above a certain critical value of z_{Se} . The lowest critical value of 1.18 Å is found for the stripe ordering (\mathbf{Q}_M). The isoline in the KS-susceptibility map (Fig. 2) begins at this critical point and shows that for the structures with other wave vectors the transition to the magnetic state takes place for larger z_{Se} . The large magnetic susceptibility at the M point for values of z_{Se} above 0.88 Å can be related to the presence of the sheets of the paramagnetic FS centered around Γ and M points. The magnetic field with wave vector \mathbf{Q}_M leads to a

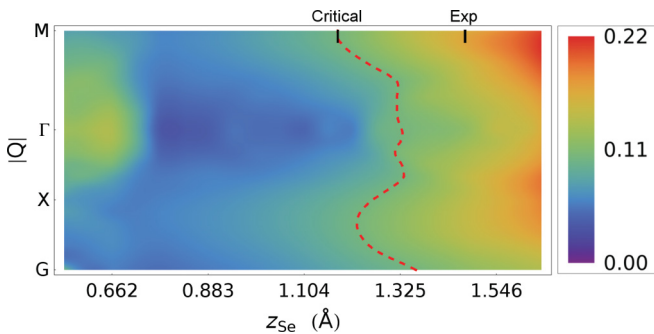


FIG. 2. (Color online) Fourier component of the static nonuniform spin susceptibility for different wave vectors \mathbf{Q} and z_{Se} . The coordinates of the symmetry points are $M = (\frac{\pi}{a}, \frac{\pi}{a}, 0)$, $X = (\frac{\pi}{a}, 0, 0)$, and $G = (\frac{2\pi}{a}, 0, 0)$.

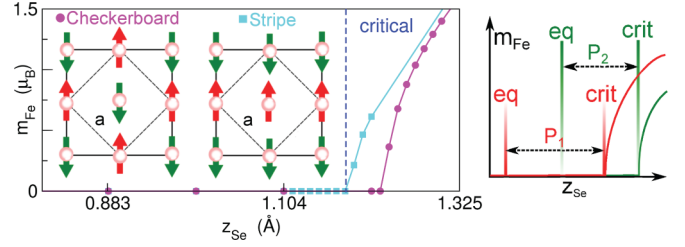


FIG. 3. (Color online) Left: Fe spin moment as a function of z_{Se} for checkerboard and stripe magnetic structures. Right: Schematic picture of the critical (crit) and equilibrium (eq) Se positions for two different pressures P_1 and P_2 ($P_1 < P_2$).

strong hybridization between two groups of states that results in considerable contribution to the induced moment.

Note that the calculated critical value of z_{Se} is smaller than the experimental¹³ z_{Se} , demonstrating that the LSDA calculations underestimate the critical z_{Se} in the case of FeSe. A possible explanation for the difference between the theoretical and experimental magnetic ground states for the experimental value of z_{Se} is the influence of zero-temperature SFs. These fluctuations are not taken into account in the LSDA functional, while close to the point of a magnetic instability they become of fundamental importance.¹⁴ It is not the purpose of this work to improve the description of the magnetic ground state by means of the account for zero-temperature SFs. This is an important nontrivial problem demanding separate consideration.

The identification of the eigenmodes of spin excitations can be performed through the diagonalization of the loss matrix, $\chi_L = \frac{i}{2}(\chi - \chi^\dagger)$.¹⁰ A nonzero eigenvalue v_λ of χ_L at a given $\mathbf{q}\omega$ signifies the presence of an excited spin state with this momentum and energy, whereas the corresponding eigenvector ξ_λ gives the shape of the associated oscillating magnetization density. In Fig. 4 we show the largest eigenvalue of the loss matrix.

Far from the critical point ($z_{\text{Se}} = 0.662$ Å), the eigenvalues of both the KS and enhanced loss matrix are small [Figs. 4(a) and 4(b)]. Coming closer to the magnetic instability ($z_{\text{Se}} = 0.994$ Å) the spectrum of the KS loss matrix changes strongly, showing a characteristic peaked structure of intense Stoner excitations. For low frequencies the intense excitations are shown at small wave vectors close to the Γ point. With increasing frequency the peaks move to larger momenta. Also the spectrum of the enhanced susceptibility evolves. Here the emerging peaks signify the formation of collective excitations [Fig. 4(d)]. The step to $z_{\text{Se}} = 1.104$ Å does not lead to a strong change in the spectral structure of the KS loss matrix [cf. Figs. 4(c) and 4(e)]. The effect on the enhanced susceptibility spectrum is, however, very strong [cf. Figs. 4(d) and 4(f)], revealing the sensitivity of the collective modes to the details of the electronic structure. The system nears now the quantum critical point and features intense spin fluctuations. The peaks correspond to collective spin excitations in the PM phase, i.e., the paramagnons. Note that the long-lived paramagnons form in the region of the q - ω plane, where the density of Stoner excitations is low. A similar effect is known for the magnon excitations in magnetically ordered systems:

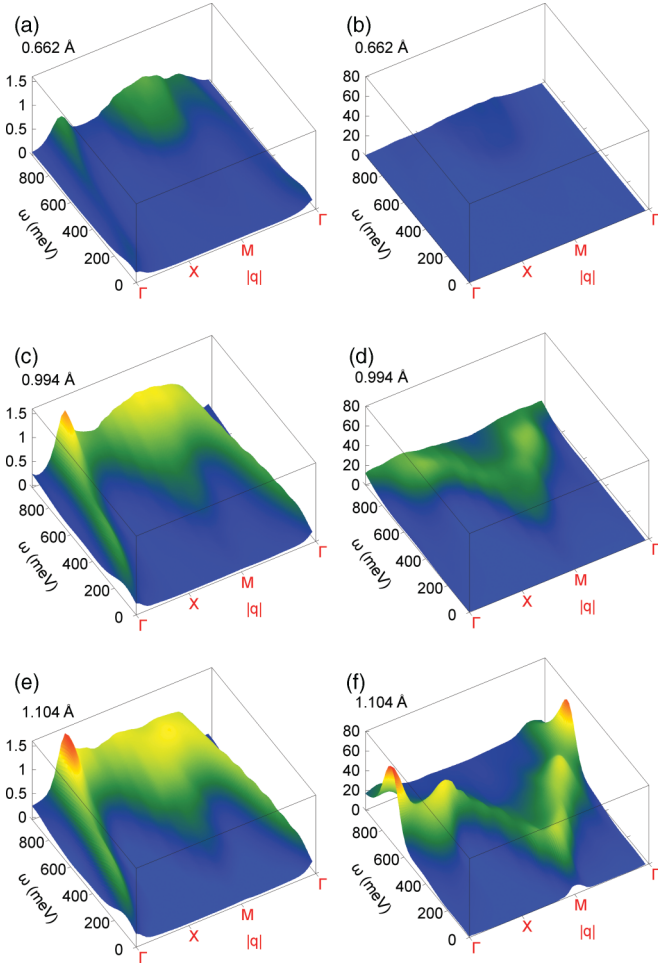


FIG. 4. (Color online) Spectral function for Stoner and collective excitations for three different z_{Se} in the PM phase. Corresponding real parts of the susceptibilities are given in the Supplemental Material (Ref. 15).

Long-living magnons can form only in the region of the q - ω plane with low intensity of Stoner transitions.¹⁰

The inspection of the spectrum [Fig. 4(f)] shows that no paramagnons form below 160 meV. This feature reveals a principal difference between magnons and paramagnons. Due to the spontaneously broken spin rotational symmetry in ordered magnets, the magnons satisfy the condition of the Goldstone theorem, this means that at least one magnon mode evolves from the point $|\mathbf{q}| = \omega = 0$. On the other hand, paramagnons are longitudinal fluctuations and a Goldstone mode does not form. The magnon spectrum calculated for the stripe AFM structure with four Fe atoms in the unit cell is shown in Fig. 5. The two magnon branches are double degenerate. As mentioned above, the magnons satisfy the Goldstone theorem and, therefore, there is a branch with magnon energy tending to 0 for $|\mathbf{q}| \rightarrow 0$.

To better understand the nature of the excitations in the PM phase, we consider the spatial distribution of the magnetization corresponding to the paramagnons (Fig. 6). This information is straightforwardly obtained from the analysis of the eigenvectors ξ_{λ} of the loss matrix. The magnetization for three \mathbf{q} vectors corresponding to the high symmetry

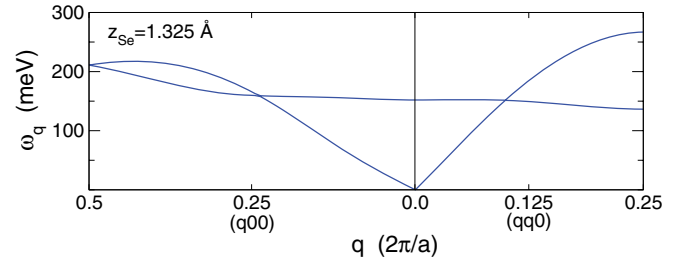


FIG. 5. (Color online) Magnon spectrum in the AFM phase.

points is shown in Fig. 6. In general, the spin magnetization is predominantly localized around Fe atoms. Therefore the properties of the paramagnons can be discussed in terms of magnetic moments m_i^z associated with Fe atoms. The variation of m_i^z is proportional to $\cos[\omega_{\mathbf{q}}t + \phi_{\mathbf{q}}(\mathbf{r}_i^{\text{Fe}}) + \mathbf{q}\mathbf{T}]$, where $\omega_{\mathbf{q}}$ is the frequency and $\phi_{\mathbf{q}}(\mathbf{r}_i^{\text{Fe}})$ the phase of the paramagnon. The \mathbf{r}_i^{Fe} ($i = 1, 2$) are the positions of Fe atoms within the unit cell and \mathbf{T} is a lattice translation.

For the lowest-energy paramagnon corresponding to the M point the Fe moments oscillate in phase, i.e., $\Delta\phi_{\mathbf{q}M} = \phi_{\mathbf{q}M}(\mathbf{r}_1^{\text{Fe}}) - \phi_{\mathbf{q}M}(\mathbf{r}_2^{\text{Fe}}) = 0$. The distribution of the moments at different atoms reflects the stripe AFM structure [Fig. 6(a)]. For the paramagnon at the X point the oscillations on the two Fe sites are out of phase by 90° [Fig. 6(c)]. In analogy with phonons, we can refer to the excitations with smaller phase between the moments as acoustic paramagnons and to the excitations with larger phase as optical paramagnons. The high-energy paramagnon corresponding to the Γ point has an

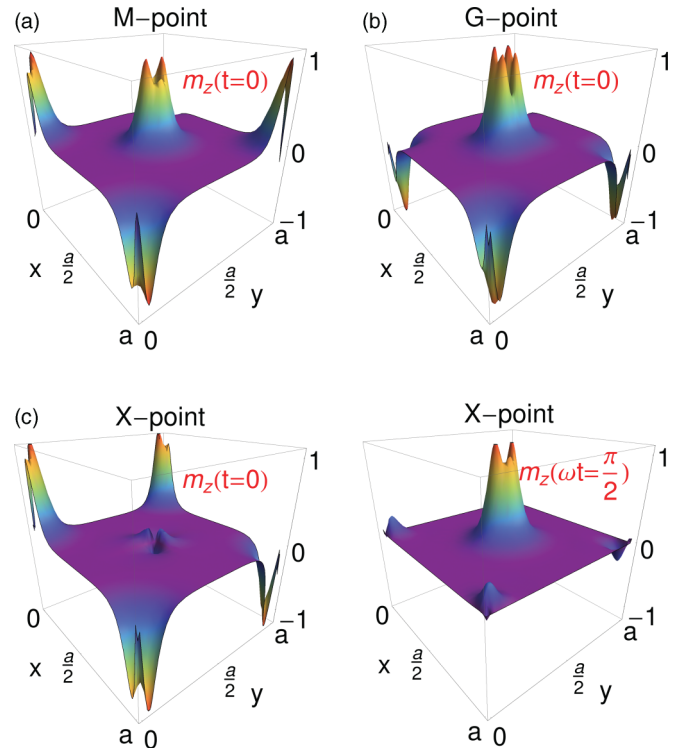


FIG. 6. (Color online) The spatial distribution of spin magnetization for three paramagnons corresponding to wave vectors of high symmetry.

optical character ($\Delta\phi_{\mathbf{q}_r} = 180^\circ$) and reflects the checkerboard AFM structure [Fig. 6(b)].

Recently inelastic neutron scattering measurements were reported for $\text{FeTe}_{1-x}\text{Se}_x$.¹⁶ Our current code implementation does not allow the study of disordered alloys. We notice, however, an important qualitative correlation between our results for FeSe and the measurements for $\text{FeTe}_{1-x}\text{Se}_x$. In agreement with our calculations, the paramagnons detected for wave vectors ($\mathbf{q}_M, \mathbf{q}_X, \mathbf{q}_G$) show the same order of energies, $\omega_{\mathbf{q}_M} < \omega_{\mathbf{q}_X} < \omega_{\mathbf{q}_G}$.

A problem of high importance is the physical mechanism behind the strong increase of the superconducting transition temperature with applied pressure.⁴ Obviously, before a consistent microscopic theory of the unconventional superconductivity is developed, a quantitative parameter-free description of this effect cannot be done. On the qualitative level, the increase of T_c is expected to be connected with further enhancement of the spin fluctuations, which is also indicated by experiment.⁴

Note that there are contradictory experimental data on the pressure dependence of z_{Se} : While some experimentalists^{17,18} argue to detect z_{Se} increasing with pressure, others¹² report an opposite trend. In terms of our model, with increasing pressure the position of the Se atoms should become closer to the critical value of z_{Se} . Our calculations show that both the equilibrium z_{Se} and the critical magnetic z_{Se} increase with pressure. However, the effect on the equilibrium position is larger than on the critical value. This suggests the qualitative picture of the pressure dependence of the relative positions of the equilibrium and critical z_{Se} shown in Fig. 3. Since for increased pressure the z_{Se} becomes closer to the critical position, the low-energy spin fluctuations are enhanced.

Effective interaction. All standard approaches to SC lead to an equation for the so-called SC gap function $\Delta_{\mathbf{k}}$ that is the order parameter of the SC phase. A possible mechanism of the Cooper pairing in unconventional SC involves the competition

between two effects: electron-electron interaction mediated by spin fluctuations and the electrostatic Coulomb repulsion.¹⁹ The two interactions enter the equation for $\Delta_{\mathbf{k}}$. The insight into the SFs discussed above allows an estimation of the strength of the interaction mediated by these fluctuations. Vignale and Singwi²⁰ suggested an expression for the electron-electron interaction by means of SFs,

$$U_{\uparrow\downarrow}(\mathbf{q}) = \frac{2}{\pi} f^{xc}(\mathbf{q}) \int d\omega \frac{\text{Im}[\chi_{zz}(\mathbf{q}\omega)]}{\omega} f^{xc}(\mathbf{q}). \quad (2)$$

To estimate the value of the interaction we evaluate matrix elements of $U_{\uparrow\downarrow}$ with respect to the KS wave functions. The largest matrix elements are obtained for momentum transfer close to \mathbf{q}_M corresponding to the lowest-energy paramagnon excitations [Fig. 4(f)]. The maximal estimated value is ~ 0.8 eV. It corresponds to the electron scattering between the pocket and the barrel pieces of the FM (Fig. 1). The competing Coulomb repulsion is large for small momentum transfer. For intraband scattering within the pocket FS the matrix element has a value of ~ 0.9 eV. These estimations give the same order of magnitude for the two interactions supporting the scenario of Cooper pairing mediated by SFs.

Summary. We report a first-principles study of the magnetic excitations in FeSe for both PM and AFM phases. The position of the selenide layer is varied to model the quantum phase transition $\text{PM} \leftrightarrow \text{AFM}$. In the paramagnetic phase, close to the magnetic instability, we find a branch of long-lived paramagnons. We discuss the properties of the paramagnons and contrast them to the properties of the collective spin excitations in magnetically ordered systems. The strength of the effective electron-electron interaction mediated by paramagnons is estimated to be of the same order of magnitude as the screened Coulomb interaction. This supports the proposed by Mazin *et al.*⁷ of the paramagnon-driven superconductivity with a s_{\pm} gap symmetry.

Acknowledgment. We thank Antonio Sanna for stimulating discussions.

¹Y. Kamihara, T. Watanabe, M. Hirano, and H. Hosono, *J. Am. Chem. Soc.* **130**, 3296 (2008).

²T. M. McQueen, Q. Huang, V. Ksenofontov, C. Felser, Q. Xu, H. Zandbergen, Y. S. Hor, J. Allred, A. J. Williams, D. Qu, J. Checkelsky, N. P. Ong, and R. J. Cava, *Phys. Rev. B* **79**, 014522 (2009).

³A. Subedi, L. Zhang, D. J. Singh, and M. H. Du, *Phys. Rev. B* **78**, 134514 (2008).

⁴S. Medvedev, T. McQueen, I. Troyan, T. Palasyuk, M. Eremets, R. Cava, S. Naghavi, F. Casper, V. Ksenofontov, G. Wortmann, and C. Felser, *Nat. Mater.* **8**, 630 (2009).

⁵T. Imai, K. Ahilan, F. L. Ning, T. M. McQueen, and R. J. Cava, *Phys. Rev. Lett.* **102**, 177005 (2009).

⁶L. Boeri, O. V. Dolgov, and A. A. Golubov, *Phys. Rev. Lett.* **101**, 026403 (2008).

⁷I. I. Mazin, D. J. Singh, M. D. Johannes, and M. H. Du, *Phys. Rev. Lett.* **101**, 057003 (2008).

⁸E. K. U. Gross and W. Kohn, *Phys. Rev. Lett.* **55**, 2850 (1985).

⁹P. Buczek, A. Ernst, P. Bruno, and L. M. Sandratskii, *Phys. Rev. Lett.* **102**, 247206 (2009).

¹⁰P. Buczek, A. Ernst, and L. M. Sandratskii, *Phys. Rev. B* **84**, 174418 (2011).

¹¹G. Fischer, M. Däne, A. Ernst, P. Bruno, M. Lüders, Z. Szotek, W. Temmerman, and W. Hergert, *Phys. Rev. B* **80**, 014408 (2009).

¹²S. Margadonna, Y. Takabayashi, Y. Ohishi, Y. Mizuguchi, Y. Takano, T. Kagayama, T. Nakagawa, M. Takata, and K. Prassides, *Phys. Rev. B* **80**, 064506 (2009).

¹³T. M. McQueen, A. J. Williams, P. W. Stephens, J. Tao, Y. Zhu, V. Ksenofontov, F. Casper, C. Felser, and R. J. Cava, *Phys. Rev. Lett.* **103**, 057002 (2009).

¹⁴A. Aguayo, I. I. Mazin, and D. J. Singh, *Phys. Rev. Lett.* **92**, 147201 (2004).

¹⁵See the Supplemental Material at <http://link.aps.org/supplemental/10.1103/PhysRevB.86.060412> for the corresponding real parts of the susceptibilities shown in Fig. 4.

¹⁶M. D. Lumsden, A. D. Christianson, E. A. Goremychkin, S. E. Nagler, H. A. Mook, M. B. Stone, D. L. Abernathy, T. Guidi,

- G. J. MacDougall, C. de la Cruz, A. S. Sefat, M. A. McGuire, B. C. Sales, and D. Mandrus, *Nat. Phys.* **6**, 182 (2010).
- ¹⁷R. Kumar, Y. Zhang, S. Sinogeikin, Y. Xiao, S. Kumar, P. Chow, A. Cornelius, and C. Chen, *J. Phys. Chem. B* **114**, 12597 (2010).
- ¹⁸J. N. Millican, D. Phelan, E. L. Thomas, J. B. Leão, and E. Carpenter, *Solid State Commun.* **149**, 707 (2009).
- ¹⁹D. Manske, *Theory of Unconventional Superconductors* (Springer, Heidelberg, 2008).
- ²⁰G. Vignale and K. S. Singwi, *Phys. Rev. B* **32**, 2156 (1985).